Research Square

Preprints are preliminary reports that have not undergone peer review.
They should not be considered conclusive, used to inform clinical practice,
or referenced by the media as validated information.

Tissue Paper-based Composite Separator Using Nano-SiO_2 Hybrid Crosslinked Polymer Electrolyte as Coating Layer For Lithium Ion Battery With Superior Security and Cycle Stability

Xinyu Zeng
Wuhan Textile University
Yu Liu
Wuhan Textile University
Rulei He
Wuhan Textile University
Tongyuan Li
Wuhan Textile University
Yuqin Hu
Wuhan Textile University
Cheng Wang
Wuhan Textile University
Jing Xu (jingxu@wtu.edu.cn)
Wuhan Textile University https://orcid.org/0000-0003-3823-7428
Luoxin Wang
Wuhan Textile University
Hua Wang
Wuhan Textile University

Research Article

Keywords: Lithium ion battery, Composite separator, Paper, Crosslinked network

Posted Date: November 23rd, 2021

DOI: https://doi.org/10.21203/rs.3.rs-1038574/v1

License: This work is licensed under a Creative Commons Attribution 4.0 International License.
Read Full License

Version of Record: A version of this preprint was published at Cellulose on March 16th, 2022. See the published version at https://doi.org/10.1007/s10570-022-04499-5.

Abstract

With the development of energy-storage devices, separator is encountered by several challenges including adequate safety, higher current density and superior stability. Tissue paper, composed of packed cellulose fibers, possesses lower production cost, more easily accessibility, superior wettability and outstanding thermostability, thus being prospective as a substrate of high performance separator. To address structure collapse phenomenon occurred in conventional coating layer after long term electrolyte swelling, nano-SiO_2 hybrid crosslinked network was constructed on tissue paper through chemical reactions between polymer poly (vinylidene fluoride-co-hexafluoropropylene) (PVDF-HFP) and hyperbranched polyethyleneimine (PEI) in this work. The influences of crosslinking degree on physical properties and electrochemical performance were studied thoroughly. It can be found that when the crosslinking ratio of PVDF-HFP and PEI fixed at 10:1, the crosslinked composite separator displays excellent electrolyte uptake and wettability, superior ionic conductivity, better interfacial compatibility as well as higher Li^+ transference number (0.56), thus offering battery with prominent rate capabilities. Besides, this crosslinked composite separator exhibits satisfying dimensional stability even treated at 250 ^oC, better flame retardancy, enhanced mechanical behavior, wider electrochemical window and outstanding cycle stability. Accordingly, tissue paper-based crosslinked composite separator can meet higher requirements put forward by high power lithium ion battery.

Highlights

- Tissue paper was employed to fabricate lithium ion battery separator.
- Nano-SiO_2 hybrid crosslinked polymer electrolyte was constructed to modify tissue paper.
- The composite separator gave superior electrochemical performance and prominent rate capabilities.
- The designed coating layer was confirmed to increase mechanical strength, broaden electrochemical window and maintain cycle stability obviously.
- Excellent thermal stability and certain self-extinguishing were obtained for composite separator to afford security.

1. Introduction

Due to high energy density, low self-discharge, long cycle life, no memory effect and so on, lithium ion battery (LIB) has not only dominated the 3C industry, but also developed into energy storge area and electric vehicles in recent years. This puts forward higher requirements to the components of LIB including higher current density, superior security as well as sufficient stability (Li, Yu, Hu, & Hu, 2020; Waqas et al., 2019). Traditional polyolefin membranes has been a widely used separator, which can isolate the positive and negative electrodes to prevent from short circuit meanwhile must allow lithium ion transport to maintain normal operation of battery. However, some drawbacks cannot be ignored such

as lower porosity, poorer electrolyte wettability and worse heat tolerance, which make polyolefin membranes meet abovementioned high performance difficultly (Yuan et al., 2021).

Fibrous membrane fabricated by nonwoven technology has superior porosity, and can realize its thermoresistance through the choice of materials, thus being considered as development trend of power battery separator in the future (E. Wang, Chiu, & Chou, 2020). So far, some types of high performance engineering plastic have been widely employed to prepare nonwoven fabric, for example polyphenylene sulfide (J. Zhang et al., 2020), polyimide (Rodriguez et al., 2021) and aramid (C. Zhu et al., 2019). However, there are some shortcomings including high cost, complicated manufacture process and poor wettability belonged to these synthetic polymers. Cellulose is the most abundant natural polymer in nature, and owns good hydrophilicity and prominent thermal stability (Huang, 2014; J. Zhang et al., 2013). Tissue paper, as a common kind of cellulose nonwoven product, can be obtained conveniently and cheaply. Accordingly, more attention has been paid by scientists to explore the potential of tissue paper based separator applied in high power LIB (Jia et al., 2020; Z. Wang et al., 2018).

As a result of some inherent defects such as larger pore size, weaker mechanical strength and poorer flame retardancy, tissue paper cannot be directly employed as LIB separator unless experienced modification (Z. Wang et al., 2018). Single polymer such as poly (vinylidene fluoride-co-hexafluoropropylene) (PVDF-HFP) or styrene-butadiene rubber (SBR) has been widely reported as binder to adhere nanoparticles on substrate (Luo et al., 2018; Y. Zhang, Wang, Xiang, Shi, & Wang, 2016). However, this binder would be swollen by electrolyte during long term cycling, thus causing nanoparticles shedding from the substrate gradually. This would further bring about the occurrence of internal short circuit and even sudden attenuation of cell performance. In our previous study, 3D crosslinked network has been constructed as a coating layer to decorate PPS nonwoven fabric (J. Zhang et al., 2020; C. Zhu et al., 2020). Superior cycle stability and enhanced mechanical strength were obtained when compared with traditional design. This envision us to attempt the employment of crosslinked binder fixing nanoparticles on tissue paper, so that making up existing deficiency and satisfying those demands raised by energy storage devices. Moreover, it is very worthwhile to study the relationship of its crosslinking ratios with physical structure and electrochemical performance.

In this study, nano-SiO_2 hybrid crosslinked coating layer through chemical reactions between polymer poly (vinylidene fluoride-co-hexafluoropropylene) (PVDF-HFP) and hyperbranched polyethyleneimine (PEI) was constructed on tissue paper. Among them, nano-SiO_2 was mainly utilized to improve flame resistance. Hyperbranched PEI could fix carbonate electrolyte *via* H-bonding, embed more electrolyte using its internal cavities and promote the swelling of electrolyte through serious crystal disruption from its steric molecular structure (Y.-H. Zhao, Xu, & Zhu, 2009). Besides, primary amine groups of PEI and C-F bonds in PVDF-HFP would produce chemical reactions so that giving a crosslinked network (R. Zhou et al., 2014). We did a series of tests related to separators including structural identification, surface morphology and pore structure, electrolyte uptake and wettability, thermal analysis and mechanical behavior as well as electrochemical and cell performance. To evaluate the performance of crosslinked composite separator, Celgard 2400 and traditional composite separator using PVDF-HFP and nano-SiO_2

as a coating layer of tissue paper were together chosen as control groups. Especially, we changed the crosslinking ratios between PVDF-HFP and PEI during membrane preparation, thoroughly discussed their effects on abovementioned properties and established corresponding correlations.

2. Experimental

2.1 Materials

Vinda tissue paper was purchased and employed as a substrate after hot pressed at 30 Mpa. Poly(vinylidene fluoride-co-hexafluoropropylene) (PVDF-HFP, M_w = 400000) and hyperbranched polyethylenimine (PEI, M_w = 25000) were purchased from Sigma-Aldrich. Nano-SiO_2 (30 nm) was obtained from Shanghai Macklin Biochemical Co., Ltd. Acetone and *N*, *N*-dimethylformamide (DMF) were supplied by Sinopharm Chemical Reagent Co., Ltd. 1 M lithium hexafluorophosphate ($LiPF_6$) in ethylene carbonate (EC)/dimethyl carbonate (DMC) (1/1, v/v) was provided by Nanjing Mojiesi Energy Technology Co., Ltd as liquid electrolyte. Lithium iron phosphate ($LiFePO_4$) and lithium metal anodes were purchased from Shenzhen Kejing Star Technology Co., Ltd.

2.2 Preparation of paper-based composite separator

PVDF-HFP and nano-SiO_2 were firstly dissolved in a solvent mixture of acetone and DMF (v/v, 4:1) by ultrasonic. Then, PEI was added into this solution at room temperature and stirred for 30 min, through which pre-crosslinked structure would be formed in the coating solution according to previous literatures (R. Zhou et al., 2014; R. Zhou, Liu, Yao, Leong, & Lu, 2015). The final ratio of PVDF-HFP : PEI : SiO_2 : solvent was set as 1 : X : 0.2 : 10 (X=0, 0.05, 0.1, 0.2, 0.4). Next, the pretreated tissue paper was respectively dipped into a series of solutions as described above and the excess coating solution was removed by blade after paper fetched out. The coated membrane was dried in air and then placed in vacuum oven at 60°C for 12 h to evaporate residual solvent completely along with subsequence crosslinking reactions between PVDF-HFP and PEI. These membranes were finally hot pressed under the condition of 60 ^oC, 10 Mpa to make the surface smooth. The obtained composite separators with different crosslinking ratios were respectively abbreviated as CS(1:0), CS(20:1), CS(10:1), CS(5:1), CS(5:2) separators. CS(1:0) separator was the traditional composite separator only using PVDF-HFP and nano-SiO_2 as coating layer and chosen as a control group in this study.

2.3 Physical characterization and measurement

Attenuated total reflection fourier transform infrared (ATR-FTIR) spectra of composite membranes were scanned on infrared spectrometer (BRUKER TENSOR-27 TGA-IR) at a wave number ranging from 600 to 4000 cm^{-1}. A scanning electron microscopy (SEM, JEOL JSM-6510LV) was employed to examine surface morphologies of composite separators after gold sputtering treatment on samples. The pore size and distribution of separator was characterized by capillary flow aperture analyzer (CFP,PMI,CFP-1500-AEXL). The porosity of separator was estimated by *n*-butyl alcohol immersion method and calculated using Eq. 1:

$$Porosity = \frac{W_{wet} - W_{dry}}{\rho_b V_p} \times 100\% (1)$$

where W_{dry} and W_{wet} are respectively the mass of sample before and after immersed in *n*-butyl alcohol for 1 h, ρ_b is the density of *n*-butyl alcohol, and V_p is the volume of dry sample.

Contact Angle tester (FM40 Easy Drop, KRUSS) was carried out to measure the static contact Angle of electrolyte droplet (2 μL) on the surface of the membrane. Macroscopically, the capillary absorption height was also measured after immersing one end of the sample in electrolyte about 2 h. In addition, separators were fully immersed in the electrolyte for 2 h, and when excess electrolyte were absorbed by filter paper, electrolyte uptake could be calculated according to Eq. 2:

$$Electrolyteuptake = \frac{W_{wet} - W_{dry}}{W_{dry}} \times 100\% (2)$$

where W_{wet} and W_{dry} are respectively the mass before and after separator immersed in the electrolyte. Thermal dimensional stabilities of membranes were identified by heat treatment at different temperatures from 50°C to 250°C. In addition, combustion tests were conducted to characterize flame retardant properties of membranes. Differential scanning calorimetry (DSC, 204 F1 NETZSCH) was employed to analysis thermal properties at the temperature range of 20°C – 300°C with a heating rate of 10°C/min. Mechanical behavior was tested with a universal testing machine (Instron-5967, USA) at room temperature. The strain rate of the machine was set at 10 mm/min and the standard sample was cut at 4 mm in width and 15 mm in length.

2.4 Electrochemical analysis

Nyquist plots of symmetrical cells (SS/separator/SS, SS = stainless-steel sheets) were gained by scanning electrochemical impedance spectroscopy (EIS) on an electrochemical workstation (Ivium Stat.h) with an AC voltage of 10 mV amplitude in the frequency range of 0.1 to 10^6 Hz. The ionic conductivity (δ) could be calculated with Eq. 3:

$$\delta = \frac{d}{RA} (3)$$

where *d* and *A* respectively represent the thickness and effective testing area of separator, and *R* is the bulk resistance of separator and obtained from Nyquist plots.
To analyze interfacial resistance between separator and electrode, electrochemical impedance spectroscopy (EIS) of symmetrical cells (Li/separator/Li) were measured on an electrochemical workstation (Ivium Stat.h) through the same way as above. In addition, we combined chronoamperometry and electrochemical impedance spectra (EIS) of Li/separator/Li cell to estimate lithium ion transference number according to Eq. 4:

$$t_{Li^+} = \frac{I_{ss}\Delta V - I_0 I_{ss} R_0}{I_0 \Delta V - I_0 I_{ss} R_{ss}} (4)$$

wherein, I_0 and I_{ss} are the initial and steady-state current obtained from chronoamperometry, respectively; R_0 and R_{ss} are the initial and steady-state interfacial resistance acquired from EIS, respectively; ΔV is the step potential difference (10 mV). Moreover, SS/separator/Li cells were assembled to evaluate electrochemical stability window of separator through linear sweep voltammetry (LSV) measurement with the potential scanned from 2.0 to 6.0 V under a rate of 10 mV/s.

2.5 Cell assembly and performance characterization

2016-type coin cell was assembled in an argon filled glove box by sandwiching liquid electrolyte-soaked separator between a $LiFePO_4$ cathode and a lithium foil anode. $LiFePO_4$ cathodes were prepared by coating NMP-based mixture of acetylene black, polyvinylidene fluoride and $LiFePO_4$ (1:1:8 by weight) on aluminum foils in our lab. Cell performance was tested on a LAND battery testing system (CT2001A, Wuhan LAND Electronic Co., Ltd, China) with the cut-off voltage range set from 2.5 to 4.2 V. In the tests of rate capabilities, these cells were charged at 0.2 C rate and discharged at various rates ranging from 0.2 to 2 C and then back to 0.2 C. At each rate the cells were charged/discharged for 10 times. During cycling tests, these cells were cycled at a fixed charge/discharge current density 0.5 C/0.5 C for 100 times at room temperature.

3. Results And Discussion

3.1 Crosslinked structure fabricated on tissue paper

Figure 1(a) describes the procedure of nano-SiO_2 hybrid crosslinked coating layer constructed on tissue paper. Firstly, polymer poly(vinylidene fluoride-co-hexafluoropropylene) (PVDF-HFP), hyperbranched polyethyleneimine (PEI) and nanoparticle SiO_2 were well mixed in solvent with a series of different ratios at room temperature, meanwhile pre-crosslinking structure would be produced. Then, a certain size tissue paper was dipped into the pre-crosslinking coating solution. The final composite separators with different crosslinking ratios were obtained after experienced vacuum drying at 60 ^oC. It should be pointed out that crosslinking reactions were occurred between -NH_2 groups in PEI and VDF segments in PVDF-HFP. As reported in previous literatures (Taguet, Ameduri, & Dufresne, 2006; R. Zhou et al., 2014; R. Zhou et al., 2015), VDF segments could take off HF molecules through autocatalytic effect of basic amines to form -CF=CH- bonds. Afterwards, due to electron withdrawing effect of F atoms in -CF=CH- groups and nucleophilicity of amines, michael addition reactions would take place between them to create new bonds. This structure would continue to suffer from rearrangement, finally leading to the formation of C=N bonds. ATR-FTIR spectra were carried out to detect this generation and shown in Figure 1(b). Though similar absorption peaks appear in the two composite separators whether crosslinked or not, there is still a characteristic absorption peak at 1642cm^{-1} distinguished for separator CS(10:1), corresponding to C=N stretching vibration and indicating the successful occurrence of crosslinking reactions between PEI and

PVDF-HFP. In addition, another two different bands centered at 1565cm^{-1} and 1476cm^{-1} can be discovered in CS(10:1) curve, which are respectively assigned to the N–H bending vibration of unreacted primary amine groups and the N–H deformative vibration of secondary amine groups in PEI (Chen, Chen, Liu, Zhao, & Wang, 2019; Chuang, Lin, Wang, & Hong, 2021). The existence of crosslinked network will produce a steady reticular structure to endure external force. As displayed in subsequent results (Fig. 3(d)), significant enhancement of tensile strength can be observed after PEI added into the composite separator, which further provides supporting evidence for the occurrence of crosslinking reactions in this system (Shin et al., 2021).

3.2 Morphology and pore structure

The separator sandwiched between two electrodes not only plays an important role in physical isolation, but also requires appropriate pores to allow rapid transmission of lithium ions in the battery (Yang, Shi, Chu, Shao, & Wang, 2021). SEM is usually employed to detect information about surface morphology and pore structure. As seen in Fig. 1(c) and 1(d), tissue paper is made from a disorderly stack of fibers, which results in apertures ranging from a few microns to dozens of microns and distributed non-uniformly. To avoid short-circuit phenomenon and heterogeneous lithium deposition, it is imperative to give a modification for tissue paper. Accordingly, nano-SiO_2 hybrid crosslinked polymer coating was introduced on the surface of tissue substrate and the final thickness of CS(10:1) separator was about 56 μm, as shown in cross section SEM (Fig. S1). Compared with CS(1:0) separator only using nano-SiO_2 hybrid PVDF-HFP as coating layer (Fig. 1(e-f)), CS(10:1) separator was observed from Fig. 1(g-h) gives more highly interconnected three-dimensional hole structures, which will provide unobstructed access for lithium ion transmission (Yang et al., 2021). Notably, these structures also present with differently size, among which the larger pores can be benefit to contain a large number of electrolytes and the smaller pores can be advantage to prevent the penetration of lithium dendrite (Lopez, Mackanic, Cui, & Bao, 2019). The quantitative data of pore size distribution of separators were measured and shown in Fig. 1(i). We can find that the pore size of CS(1:0) separator is basically concentrated at about 1 μm, while three interval distributions are presented for CS(10:1) separator using crosslinked system as coating layer and respectively placed at 1.2, 0.9 and 0.5 μm. This result is consistent with pore structure observed from SEM images. Because of smaller size as dominant, the even pore size of CS(10:1) separator is about 0.65 μm, lower than that of CS(1:0) separator. These results can be attributed to the introduction of hyperbranched PEI and the formation of crosslinked structure between PEI and PVDF-HFP, which can decrease crystallinity of polymer matrix, change distances between polymer chains and further realize the regulation of pore size (L. Liu et al., 2021).

The capacity of separator to accommodate electrolyte has a close relationship with porosity (W. Zhang et al., 2018). As shown in Table 1, with the increase of crosslinking agent PEI, the porosity of crosslinked composite separator gradually decreases, but much higher than that of Celgard 2400 (30%). When fixing the ratio of PVDF-HFP and PEI at 20:1 or 10:1, the porosity of about 70% can be obtained, which is basically similar with that of traditional composite separator CS(1:0). This demonstrates higher porosity and smaller pore size can simultaneously achieve through controlling the crosslinking ratio, which are the

prerequisite for absorbing more electrolytes and preventing the penetration of lithium dendrite (Guan et al., 2020).

Table 1
Basic properties of Celgard 2400 and composite separators.

Separator	Porosity (%)	Electrolyte uptake (%)	Ion conductivity (mS/cm)
Celgard 2400	30	70	0.19
CS(1:0)	77	227	0.57
CS(20:1)	73	248	0.65
CS(10:1)	71	254	0.69
CS(5:1)	66	236	0.51
CS(5:2)	58	229	0.43

3.3 Wettability and electrolyte uptake

Wettability can reflect adsorption and expansion rate of electrolyte on separator (Lv et al., 2021). Fig. 2(a) gives immersion-height photograph at the time of separator immersed in liquid electrolyte 120 min. It was found that with the increase of hyperbranched PEI content, electrolyte immersion-height for the crosslinked composite separator raised firstly and then reduced. When the crosslinking ratio of PVDF-HFP and PEI was set at 10:1, highest immersion-height achieved with the value of 3.2 cm. As a comparison, only 0.3 cm and 2.2 cm immersion-height were respectively obtained for Celgard 2400 and the control CS(1:0) separator. This behavior demonstrates superior wettability of CS(10:1) separator. Moreover, contact angles of electrolyte on separators were measured and shown in Fig. 2(b). Compared with Celgard 2400 and CS(1:0) separator, the lowest contact angle was obtained for CS(10:1) separator no matter at initial contact or after 20 S. As the crosslinking degree increased, there were complete opposite trends observed between contact angle and immersion-height, indicating coincident wettability results. These results can be attributed to hydrophilicity of tissue paper substrate and strong polarity provided by abundant amines in hyperbranched PEI, which can improve electrolyte affinity with separator and be helpful for electrolyte adsorption (Sheng et al., 2021). On the other hand, the incorporation of crosslinking agent at an appropriate content can regulate the formation of interconnected pore structure but produce negligible effect on porosity, which can make the adsorbed electrolyte infiltrate and diffuse in separator quickly (Sheng et al., 2021). However, deeply crosslinking can hinder the penetration of electrolyte and result in attenuation of wettability, which is mainly related to the reduction of porosity as displayed in Table 1. Good wettability of CS(10:1) separator will be beneficial to lithium ion migration between electrodes especially for high power LIB and reduce standing time after cell assembly (Sheng et al., 2021).

Separator serves as electrolyte reservoir to ensure number of lithium ions transferred during battery operation, thus electrolyte uptake is an important parameter to decide electrochemical performance (Z. Zhang, Zhou, Yu, Cai, & Yang, 2020). According to data from Table 1, compared with Celgard 2400, the control composite separator CS(1:0) can accommodate more electrolyte. This behavior has a close relationship with its higher porosity and better hydrophilicity to electrolyte caused by the employment of polar coating layer (PVDF-HFP and SiO_2) and substrate (Yuan et al., 2021). With the addition of crosslinking agent PEI, the capacity to absorb electrolyte begins to increase gradually. Specially, the crosslinked composite separator CS(10:1) gives the highest electrolyte uptake with the value of 254%. This cannot separate from good affinity between strong polarity PEI and electrolyte. In addition, the application of hyperbranched PEI forming crosslinking structure can reduce the crystallinity of polymer coating PVDF-HFP, which will be advantageous to liquid electrolyte swell into coating layer (R. Zhou et al., 2015). These two factors and basically unchanged porosity endow CS(10:1) separator with promoted electrolyte uptake. As PEI content continued to increase, the electrolyte uptake of the crosslinked composite separator begins to decrease mainly due to reduced porosity displayed in Table 1. Higher electrolyte uptake of CS(10:1) separator will accommodate more Li^+ to participate in charge transfer, thus producing lower internal impedance (Yuan et al., 2021).

3.4 Thermal analysis, flame retarding property and mechanical behavior

To cope with heat generated during the operation of high power LIB, separator must have sufficient thermal stability and flame retardancy, so that providing superior safety when battery working in a variety of possible normal cases, or not causing more serious explosions when sudden short-circuit reaction occurred (Babiker et al., 2021). Fig. 3(a) gives photographs of separators experienced heat treatment at different temperatures. We can find that Celgard 2400 separator is suffered from significant dimensional shrinkage above 200°C until completely fusion. However, the original size can be kept unchanged for the prepared tissue-based composite separator in the whole temperature range. This is mainly related to cellulose, a main component of tissue paper, and nanoparticle SiO_2, which own excellent thermal stability and can afford stable supporting skeleton for composite separators (Z. Wang et al., 2018). Compared with PVDF-HFP as binder in coating layer, the introduction of crosslinked structure will also contribute to the sufficient thermal stability of composite separators, which cannot be intuitively reflected from dimensional stability. From DSC curves displayed in Fig. 3(c), we can find there is a melting peak of PVDF-HFP at about 150 ^oC for the control CS(1:0) membrane (X. Zhang et al., 2021), while no melting signal is distinguished for CS(10:1) separator with crosslinked structure. This demonstrates that the construction of crosslinked network can restrict the melting of PVDF-HFP, thus boosting heat resistance of the overall structure again (Y. Zhu, Cao, Chen, Yu, & Li, 2019). However, the color is observed to get darker gradually for the crosslinked composite separator with the increase of PEI content and heating temperature from Fig. 3(a). This phenomenon can be explained as further deepened crosslinking reactions and oxidation of unreacted amine groups in PEI (Y.-H. Zhao et al., 2009). TGA curves were also measured and shown in Fig. S2 Compared with separator CS(1:0) without SiO_2, the incorporation of

crosslinked network is observed to give composite separator with higher solid residue when temperature increased above to 600 ^{o}C. Especially, the addition of SiO_2 further raises this value and offers CS(10:1) separator with best thermal stability. By comparison, Celgard 2400 separator leaves no solid basically when temperature rising to 500 ^{o}C. Flame retardancy was tested by combustion experiment and given in Fig. 3(b). A huge difference phenomenon can be discovered when separators are approached to fire. Celgard 2400 burned and shrunk rapidly resulted from inherent thermal sensitivity and inflammability nature of polyolefin, pure tissue paper also gives a violent combustion, while the composite separator whether crosslinked or not shows self-extinguishing phenomenon. Limiting oxygen index (LOI) dates were tested and shown in Fig. S3, LOI value is observed to increase in the order of Tissue paper < CS(1:0) without SiO_2 < CS(10:1) without SiO_2 < CS(10:1). This demonstrates the addition of nano-SiO_2, the existence of fluorine element in coating layer and the fabrication of crosslinked network have synergetic effect in improving flame retardancy of CS(10:1) separator (X. Zhang et al., 2021). These behaviors will be helpful for the improvement of battery safety.

Separator should achieve certain mechanical property to meet winding operation in the production process and resist the growth of lithium dendrite during battery cycling (Wu, Ning, Jiang, Shi, & Huang, 2019). The stress-strain curves were carried out and displayed in Fig. 3(d). It can be found that pure tissue paper has a very low tensile strength of 2.9 MPa. After PVDF-HFP and SiO_2 coated on tissue paper, enhanced tensile strength (7.5 MPa) is obtained for CS(1:0) separator. Especially, when PEI also introduced in coating layer, tensile strength is increased substantially and CS(10:1) separator displays the maximum value of about 9.9 MPa. This can be ascribed to the formation of 3D crosslinked network between PVDF-HFP and PEI, which is hard to deform when suffered from external force (Chuang et al., 2021). However, with the continuous increase of crosslinking degree, tensile strength begins to reduce for CS(5:1) and CS(5:2) separator. This demonstrates that excessive crosslinked structure is too firm to absorb more external energy, thus leading to the occurrence of breakage prematurely. Clearly, tensile strength can reach the maximum improvement when coating layer incorporated with a suitable crosslinking ratio. This is a very satisfactory result when compared with other coating layers reported in previous literatures (J. Zhang et al., 2020), but still lower than that of Celgard 2400 due to its special uniaxial tension process during fabrication (E. Wang et al., 2020).

3.5 Electrochemical performance

Internal resistance can determine ohmic polarization degree in battery (Hasanpoor et al., 2021). Bulk resistance of separator together with interfacial resistance between separator and electrode restrict internal impedance in this system. As shown in Fig. 4(a), the interception of Nyquist plots on X-axis increases in the order of CS(10:1)(3.5Ω) < CS(20:1)(4.2Ω) < Celgard2400(4.6Ω) < CS(1:0)(5.2Ω) < CS(5:1)(6.2Ω) < CS(5:2)(6.9Ω), demonstrating the lowest bulk resistance for CS(10:1) separator. The ionic conductivities of separators were calculated according to Eq. 3 and decreased in the sequence of CS(10:1) > CS(20:1) > CS(1:0) > CS(5:1) > CS(5:2) > Celgard2400, which was consistent with the result of contact angles. Electrolyte uptake and penetration in separator are two important factors to determine ionic conductivity, which can ensure the number and mobility of Li^+ during battery operation (Kim et al.,

2020). CS(10:1) own the highest electrolyte uptake and basically unaffected infiltration at this crosslinking ratio, thus providing outstanding ionic conductivity. As crosslinking degree deepened, the infiltration of electrolyte in separator would be suffered from reduced aperture, thus appearing the attenuation phenomenon in conductivity. Compared with Celgard 2400, all composite separators have higher ionic conductivities but bigger thicknesses. Only for CS(10:1) and CS(20:1) separator, ionic conductivity can offset negative effect by thickness, thus giving lower bulk impedance.

Interfacial compatibility between separator and electrode is another parameter to influence ohmic polarization degree and Li^+ storage capacity (H. Zhao et al., 2020). Fig. 4(b) gives interfacial impedances of simulate batteries based on Celgard 2400 or a series of composite separators. The distance between intercepts of Nyquist plots on the real axis is considered as interfacial resistance, which includes solid electrolyte interface (SEI) film impedance located at high frequency region and charger transfer impedance placed in medium or low frequency region (Xu et al., 2015). It can be found the distance between semicircle intercepts increase stepwise with a sequence of CS(10:1) < CS(20:1) < CS(5:1) < CS(5:2) < CS(1:0) < Celgard2400, indicating better interfacial compatibility existed between crosslinked composite separator and electrode. Especially when crosslinking ratio regulated at 10:1, most favorable interfacial compatibility is reached. This can be ascribed to strong binding force produced by crosslinked network to liquid electrolyte, which will reduce free electrolyte and minimize its side reactions occurred on lithium electrode, thus cutting down SEI film impedance (Lv et al., 2021). For CS(10:1) separator, more electrolyte are entrapped by crosslinked network so that thinner SEI film and lower impedance obtained. On the other hand, superior electrolyte absorption behavior of CS(10:1) separator can facilitate to form a gel layer with adhesive property at the separator/electrode interface, thus leading to closer interfacial contact and faster Li^+ transfer (H. Zhao et al., 2020). These two factors together bring about the interfacial optimization between CS(10:1) separator and electrode.

Separator after absorbing electrolyte should maintain stability within a wide voltage range to offer a higher operating potential for LIB or withstand overcharge/overdischarge (Kim et al., 2020). Electrochemical window based on SS/separator/Li cell was detected by Linear sweep voltammetry (LSV) method and the corresponding result was depicted in Fig. 4(c). It can be found that there is a sudden current increase in LSV curve when voltage increased to a certain value, which declares the occurrence of oxidation decomposition reaction in this system (Kim et al., 2020). Accordingly, initial decomposition voltages can be observed to increase in the order of Celgard2400 < CS(5:2) < CS(5:1) < CS(1:0) < CS(20:1) < CS(10:1), indicating better anodic stability for CS(10:1) separator. This behavior can be attributed to improved electrolyte storage capability and enhanced binding force between composite separator and carbonate electrolyte by the construction of crosslinked network, which can alleviate the decomposition of free solvent molecules on the anode, thus being inclined to provide broader electrochemical window for LIB (Liang, Liang, Cao, & Wu, 2021). While crosslinking degree increased, electrolyte storage capability begins to get weaker, thus resulting to the existence of more free electrolyte in cell and the earlier appearance of oxide decomposition.

Lithium ion transference number is an important parameter in investigating concentration polarization phenomenon (Zahn, Lagadec, Hess, & Wood, 2016). In this study, Li^+ transference numbers (t_{Li+}) were estimated by the combination of chronoamperometry and EIS of Li/separator/Li cells as shown in Fig. 4(d-i) and calculated by Eq. 4. We can find that t_{Li+} presents an increasing trend in the order of Celgard2400 < CS(5:2) < CS(5:1) < CS(1:0) < CS(20:1) < CS(10:1), indicating that appropriate crosslinking degree can improve lithium ion transference number. This is mainly related to physical binding produced by crosslinked network to larger ions PF_6^-, which will restrict mobility of anion and give lithium ions more chance to take part in charge transfer (Suriyakumar & Stephan, 2020). Meanwhile, nano-SiO_2 in the coating layer of composite separator can also serve as Lewis acid centers to trap electrolyte anions (K. Liu et al., 2017; D. Zhou et al., 2016). These two factors finally give a superior t_{Li+} for CS(10:1) separator compared with Celgard 2400 and traditional composite separator. However, as crosslinking degree continues to increase, there is an obvious decline observed for t_{Li+}. This can be interpreted as the loss of effective fixing to electrolyte due to the shrinkage of pore structures as discussed above, which will directly result in free movement of PF_6^- and cut down charge transfer duty of Li^+. The higher t_{Li+} for CS(10:1) separator will provide timely replenishment of Li^+ during electrode reaction and be benefit to weaken concentration polarization degree (Xia et al., 2021). According to detailed investigation and analysis, in the following study we will choose CS(10:1) separator to fabricate battery due to its outstanding physical properties and electrochemical performance.

3.6 Cell performance

Lithium ion batteries assembling with Celgard 2400, CS(1:0) or CS(10:1) separator were respectively charged at a constant current rate 0.2 C and discharged at different current rates ranging from 0.2 C to 2 C and then back to 0.2 C. As shown in Fig. 5(a-c), discharge capacities of the three systems decrease gradually with the increase of discharge C rate. This can be attributed to aggravated polarization phenomenon at a higher current density including ohmic, concentration and electrochemical polarization, which will cause the reduction of discharge voltage and shorten discharge time to less than theoretical value, thus leading to attenuated discharge capacity (Yan et al., 2020). When discharge rate varied from 2 C back to 0.2 C, compared with other two systems, the battery using CS(10:1) separator presents higher coincidence whether in discharge voltage or capacity, indicating its better reversibility in cell performance. Fig. 5(d) summarizes rate capabilities of the three systems. Superior discharge capacities are observed for CS(10:1) sample in all of the C-rate. Especially, when current rate increased to 2 C, there are substantial increase discovered in the capacity divergence between them. As discussed above, CS(10:1) separator own superior ionic conductivity, excellent interface compatibility between electrode and separator as well as higher Li^+ transference number, which will lead to lower ohmic resistance and concentration polarization existed in battery, thus giving enhanced discharge performance. The influence resulted from internal polarization will be amplified as discharge rate increased, thus the capacity difference between them becoming more pronounced (Valverde et al., 2020). This outstanding cell performance at elevated rate will provide possibility for the application of CS(10:1) separator in high power LIB.

The battery must maintain a high discharge capacity after multiple cycles, which is a premise of application (Xia et al., 2021). As shown in Fig. 5(e), 100 charge/discharge cycles were carried out at 0.5 C/0.5 C rate to evaluate cycling performance. We can find all the three systems show almost 100% coulombic efficiency. Moreover, in the initial cycles, system CS(10:1) reveals slight higher discharge capacities (about 153 mAh g^{-1}) than system CS(1:0) (about 149 mAh g^{-1}), but there is a larger capacity divergency appeared between system Celgard 2400 (about 138 mAh g^{-1}) and CS(10:1). This phenomenon is consistent with rate capabilities mentioned above. As cycling tests going on, CS(1:0) system gives a stepwise decrease phenomenon in discharge capacity. Especially a sudden drop is observed from the battery based on CS(1:0) separator with discharge capacity decreasing to 90 mAh g^{-1} when cycle number surpassed 65. Finally, LIB using CS(10:1) separator gives a discharge capacity retention about 98% after 100 cycles, much higher than that of Celgard 2400 (about 84%) and CS(1:0) system (about 64%). This can be attributed to 3D crosslinked coating layer constructed on tissue paper through hyperbranched PEI and polymer matrix PVDF-HFP, which can not only fix electrolyte firmly in separator but also provide a steady coating structure to endure long term swelling of electrolyte. These behaviors will not only ensure sufficient electrolyte for lithium ion transport but also maintain efficient physical isolation existed between electrodes during the whole cycling, thus bringing about stable cycling performance for system CS(10:1) (Xia et al., 2021). On the contrary, separator CS(1:0) only employs polymer PVDF-HFP as binder, which is easy to loss overall structure and shed from substrate after swollen by electrolyte, thus resulting in micro-short circuit occurred in the last stage and the attenuation of capacity (Jia et al., 2020).

4. Conclusions

In summary, a series of composite separators were successfully obtained through constructing nano-SiO_2 hybrid coating layer with different crosslinking ratios on tissue paper. When the crosslinking ratio of PVDF-HFP and PEI set at 10:1, superior wettability, enhanced ionic conductivity, depressed interfacial impedance and higher lithium ion transference number were obtained for the composite separator, which finally endowed battery with better rate capabilities. This can be attributed to basically unaffected porosity, improved hydrophilicity and the formulation of good interconnected pore structures along with the addition of certain hyperbranched PEI. Moreover, the crosslinked coating layer was investigated to bring about the strength of mechanical behavior, the broadening of electrochemical window and unchanged cycle performance for the composite separator, demonstrating its effect on overall structure stability when suffered from various types of external stimulations. Finally, the composite separator displayed sufficient thermal resistance and obvious flame retardant phenomenon, which had a close relationship with the employment of cellulose substrate, nano-SiO_2 and crosslinked fluorinated polymer network in this system. Therefore, this designed composite separator based on tissue paper will pave a way for the development of higher power LIB.

Declarations

Acknowledgments

This work was supported by Hubei Provincial Natural Science Foundation of China (2018CFB267), the Open Project Program of Beijing National Laboratory for Molecular Sciences (BNLMS201821), and Hubei Provincial Undergraduates' Innovation and Entrepreneurship Training Program (20210100032).

References

1. Babiker DMD, Wan C, Mansoor B, Usha ZR, Yu R, Habumugisha JC, Li L (2021) Superior lithium battery separator with extraordinary electrochemical performance and thermal stability based on hybrid UHMWPE/SiO2 nanocomposites via the scalable biaxial stretching process. Composites Part B 211. https://doi.org/10.1016/j.compositesb.2021.108658
2. Chen C, Chen F, Liu L, Zhao J, Wang F (2019) Cross-linked hyperbranched polyethylenimine as an efficient multidimensional binder for silicon anodes in lithium-ion batteries. Electrochim Acta 326. https://doi.org/10.1016/j.electacta.2019.134964
3. Chuang Y-P, Lin Y-L, Wang C-C, Hong J-L (2021) Dual Cross-Linked Polymer Networks Derived from the Hyperbranched Poly(ethyleneimine) and Poly(acrylic acid) as Efficient Binders for Silicon Anodes in Lithium-Ion Batteries. ACS Appl Energy Mater 4(2):1583–1592. https://doi.org/10.1021/acsaem.0c02802
4. Guan X, Wu Q, Zhang X, Guo X, Li C, Xu J (2020) In-situ crosslinked single ion gel polymer electrolyte with superior performances for lithium metal batteries. Chem Eng J 382. https://doi.org/10.1016/j.cej.2019.122935
5. Hasanpoor M, Eftekharnia M, Pathirana T, Pal U, Kerr R, Forsyth M, Howlett PC (2021) Understanding the Role of Separator and Electrolyte Compatibility on Lithium Metal Anode Performance Using Ionic Liquid-Based Electrolytes. ACS Appl Energy Mater. https://doi.org/10.1021/acsaem.1c01114
6. Huang X (2014) Performance evaluation of a non-woven lithium ion battery separator prepared through a paper-making process. J Power Sources 256:96–101. https://doi.org/10.1016/j.jpowsour.2014.01.080
7. Jia S, Yang S, Zhang M, Huang K, Long J, Xiao J (2020) Eco-friendly xonotlite nanowires/wood pulp fibers ceramic hybrid separators through a simple papermaking process for lithium ion battery. J Membr Sci 597. https://doi.org/10.1016/j.memsci.2019.117725
8. Kim H, Mattinen U, Guccini V, Liu H, Salazar-Alvarez G, Lindstrom RW, Cornell A (2020) Feasibility of Chemically Modified Cellulose Nanofiber Membranes as Lithium-Ion Battery Separators. ACS Appl Mater Interfaces 12(37):41211–41222. https://doi.org/10.1021/acsami.0c08820
9. Li Y, Yu L, Hu W, Hu X (2020) Thermotolerant separators for safe lithium-ion batteries under extreme conditions. J Mater Chem A 8(39):20294–20317. https://doi.org/10.1039/d0ta07511f
10. Liang T, Liang W-H, Cao J-H, Wu D-Y (2021) Enhanced Performance of High Energy Density Lithium Metal Battery with PVDF-HFP/LAGP Composite Separator. ACS Appl Energy Mater 4(3):2578–2585. https://doi.org/10.1021/acsaem.0c03162

11. Liu K, Zhuo D, Lee HW, Liu W, Lin D, Lu Y, Cui Y (2017) Extending the Life of Lithium-Based Rechargeable Batteries by Reaction of Lithium Dendrites with a Novel Silica Nanoparticle Sandwiched Separator. Adv Mater 29(4). https://doi.org/10.1002/adma.201603987
12. Liu L, Xu T, Gui X, Gao S, Sun L, Lin Q, Xu K (2021) Electrospun Silsequioxane-grafted PVDF hybrid membranes for high-performance rechargeable lithium batteries. Composites Part B 215. https://doi.org/10.1016/j.compositesb.2021.108849
13. Lopez J, Mackanic DG, Cui Y, Bao Z (2019) Designing polymers for advanced battery chemistries. Nat Rev Mater 4(5):312–330. https://doi.org/10.1038/s41578-019-0103-6
14. Luo D, Chen M, Xu J, Yin X, Wu J, Chen S, Wang H (2018) Polyphenylene sulfide nonwoven-based composite separator with superior heat-resistance and flame retardancy for high power lithium ion battery. Compos Sci Technol 157:119–125. https://doi.org/10.1016/j.compscitech.2018.01.023
15. Lv D, Chai J, Wang P, Zhu L, Liu C, Nie S, Cui G (2021) Pure cellulose lithium-ion battery separator with tunable pore size and improved working stability by cellulose nanofibrils. Carbohydr Polym 251:116975. https://doi.org/10.1016/j.carbpol.2020.116975
16. Rodriguez JR, Jokhakar D, Rao H, Lin K-W, Lo C-T, Aguirre SB, Pol VG (2021) Freestanding polyimide fiber network as thermally safer separator for high-performance Li metal batteries. Electrochim Acta 377. https://doi.org/10.1016/j.electacta.2021.138069
17. Sheng L, Xie X, Sun Z, Zhao M, Gao B, Pan J, He J (2021) Role of Separator Surface Polarity in Boosting the Lithium-Ion Transport Property for a Lithium-Based Battery. ACS Appl Energy Mater 4(5):5212–5221. https://doi.org/10.1021/acsaem.1c00737
18. Shin SC, Kim J, Modigunta JKR, Murali G, Park S, Lee S,... In, I (2021) Bio-mimicking organic-inorganic hybrid ladder-like polysilsesquioxanes as a surface modifier for polyethylene separator in lithium-ion batteries. J Membr Sci 620. https://doi.org/10.1016/j.memsci.2020.118886
19. Suriyakumar S, Stephan AM (2020) Mitigation of Polysulfide Shuttling by Interlayer/Permselective Separators in Lithium–Sulfur Batteries. ACS Appl Energy Mater 3(9):8095–8129. https://doi.org/10.1021/acsaem.0c01354
20. Taguet A, Ameduri B, Dufresne A (2006) Crosslinking and characterization of commercially available poly(VDF-co-HFP) copolymers with 2,4,4-trimethyl-1,6-hexanediamine. Eur Polym J 42(10):2549–2561. https://doi.org/10.1016/j.eurpolymj.2006.04.012
21. Valverde A, Gonçalves R, Silva MM, Wuttke S, Fidalgo-Marijuan A, Costa CM, de Fernández R (2020) Metal–Organic Framework Based PVDF Separators for High Rate Cycling Lithium-Ion Batteries. ACS Appl Energy Mater 3(12):11907–11919. https://doi.org/10.1021/acsaem.0c02044
22. Wang E, Chiu C-H, Chou P-H (2020) Safety assessment of polyolefin and nonwoven separators used in lithium-ion batteries. J Power Sources 461. https://doi.org/10.1016/j.jpowsour.2020.228148
23. Wang Z, Xiang H, Wang L, Xia R, Nie S, Chen C, Wang H (2018) A paper-supported inorganic composite separator for high-safety lithium-ion batteries. J Membr Sci 553:10–16. https://doi.org/10.1016/j.memsci.2018.02.040

24. Waqas M, Ali S, Feng C, Chen D, Han J, He W (2019) Recent Development in Separators for High-Temperature Lithium-Ion Batteries. *Small 15*(33), e1901689. https://doi.org/10.1002/smll.201901689
25. Wu S, Ning J, Jiang F, Shi J, Huang F (2019) Ceramic Nanoparticle-Decorated Melt-Electrospun PVDF Nanofiber Membrane with Enhanced Performance as a Lithium-Ion Battery Separator. ACS Omega 4(15):16309–16317. https://doi.org/10.1021/acsomega.9b01541
26. Xia H, Tang Y, Malyi OI, Zhu Z, Zhang Y, Zhang W, Chen X (2021) Deep Cycling for High-Capacity Li-Ion Batteries. Adv Mater 33(10):e2004998. https://doi.org/10.1002/adma.202004998
27. Xu W, Wang Z, Shi L, Ma Y, Yuan S, Sun L, Zhu J (2015) Layer-by-Layer Deposition of Organic-Inorganic Hybrid Multilayer on Microporous Polyethylene Separator to Enhance the Electrochemical Performance of Lithium-Ion Battery. ACS Appl Mater Interfaces 7(37):20678–20686. https://doi.org/10.1021/acsami.5b05457
28. Yan J, Liu F, Hu Z, Gao J, Zhou W, Huo H, Li L (2020) Realizing Dendrite-Free Lithium Deposition with a Composite Separator. Nano Lett 20(5):3798–3807. https://doi.org/10.1021/acs.nanolett.0c00819
29. Yang H, Shi X, Chu S, Shao Z, Wang Y (2021) Design of Block-Copolymer Nanoporous Membranes for Robust and Safer Lithium-Ion Battery Separators. Adv Sci (Weinh) 8(7):2003096. https://doi.org/10.1002/advs.202003096
30. Yuan B, Wen K, Chen D, Liu Y, Dong Y, Feng C, He W (2021) Composite Separators for Robust High Rate Lithium Ion Batteries. Adv Funct Mater. https://doi.org/10.1002/adfm.202101420
31. Zahn R, Lagadec MF, Hess M, Wood V (2016) Improving Ionic Conductivity and Lithium-Ion Transference Number in Lithium-Ion Battery Separators. ACS Appl Mater Interfaces 8(48):32637–32642. https://doi.org/10.1021/acsami.6b12085
32. Zhang J, Liu Z, Kong Q, Zhang C, Pang S, Yue L, Cui G (2013) Renewable and superior thermal-resistant cellulose-based composite nonwoven as lithium-ion battery separator. ACS Appl Mater Interfaces 5(1):128–134. https://doi.org/10.1021/am302290n
33. Zhang J, Zhu C, Xu J, Wu J, Yin X, Chen S, Li Z-C (2020) Enhanced mechanical behavior and electrochemical performance of composite separator by constructing crosslinked polymer electrolyte networks on polyphenylene sulfide nonwoven surface. J Membr Sci 597. https://doi.org/10.1016/j.memsci.2019.117622
34. Zhang W, Tu Z, Qian J, Choudhury S, Archer LA, Lu Y (2018) Design Principles of Functional Polymer Separators for High-Energy, Metal-Based Batteries. *Small 14*(11), e1703001. https://doi.org/10.1002/smll.201703001
35. Zhang X, Sun Q, Zhen C, Niu Y, Han Y, Zeng G, He W (2021) Recent progress in flame-retardant separators for safe lithium-ion batteries. Energy Storage Materials 37:628–647. https://doi.org/10.1016/j.ensm.2021.02.042
36. Zhang Y, Wang Z, Xiang H, Shi P, Wang H (2016) A thin inorganic composite separator for lithium-ion batteries. J Membr Sci 509:19–26. https://doi.org/10.1016/j.memsci.2016.02.047

37. Zhang Z, Zhou M, Yu J, Cai J, Yang Z (2020) Poly(vinylidene fluoride) Modified Commercial Paper as a Separator with Enhanced Thermal Stability and Electrolyte Affinity for Lithium-ion Battery. Energy Environ Mater. https://doi.org/10.1002/eem2.12153
38. Zhao H, Deng N, Kang W, Li Z, Wang G, Cheng B (2020) Highly multiscale structural Poly(vinylidene fluoridehexafluoropropylene) / poly-m-phenyleneisophthalamide separator with enhanced interface compatibility and uniform lithium-ion flux distribution for dendrite-proof lithium-metal batteries. Energy Storage Materials 26:334–348. https://doi.org/10.1016/j.ensm.2019.11.005
39. Zhao Y-H, Xu Y-Y, Zhu B-K (2009) Effect of amphiphilic hyperbranched-star polymer on the structure and properties of PVDF based porous polymer electrolytes. Solid State Ionics 180(32–35):1517–1524. https://doi.org/10.1016/j.ssi.2009.10.003
40. Zhou D, Liu R, He Y-B, Li F, Liu M, Li B, Kang F (2016) SiO2Hollow Nanosphere-Based Composite Solid Electrolyte for Lithium Metal Batteries to Suppress Lithium Dendrite Growth and Enhance Cycle Life. Adv Energy Mater 6(7). https://doi.org/10.1002/aenm.201502214
41. Zhou R, Liu W, Kong J, Zhou D, Ding G, Leong YW, Lu X (2014) Chemically cross-linked ultrathin electrospun poly(vinylidene fluoride-co-hexafluoropropylene) nanofibrous mats as ionic liquid host in electrochromic devices. Polymer 55(6):1520–1526. https://doi.org/10.1016/j.polymer.2014.01.047
42. Zhou R, Liu W, Yao X, Leong YW, Lu X (2015) Poly(vinylidene fluoride) nanofibrous mats with covalently attached SiO2 nanoparticles as an ionic liquid host: enhanced ion transport for electrochromic devices and lithium-ion batteries. J Mater Chem A 3(31):16040–16049. https://doi.org/10.1039/c5ta02154e
43. Zhu C, Zhang J, Xu J, Yin X, Wu J, Chen S, Wang H (2019) Aramid nanofibers/polyphenylene sulfide nonwoven composite separator fabricated through a facile papermaking method for lithium ion battery. J Membr Sci 588. https://doi.org/10.1016/j.memsci.2019.117169
44. Zhu C, Zhang J, Zeng X, Xu J, Wang L, Li ZC (2020) Semi-Interpenetrating Polymer Electrolyte as a Coating Layer Constructed on Polyphenylene Sulfide Nonwoven to Afford Superior Stability and Performance for Lithium-Ion Batteries. ChemElectroChem 7(21):4492–4500. https://doi.org/10.1002/celc.202001232
45. Zhu Y, Cao J, Chen H, Yu Q, Li B (2019) High electrochemical stability of a 3D cross-linked network PEO@nano-SiO2 composite polymer electrolyte for lithium metal batteries. J Mater Chem A 7(12):6832–6839. https://doi.org/10.1039/c9ta00560a

Figures

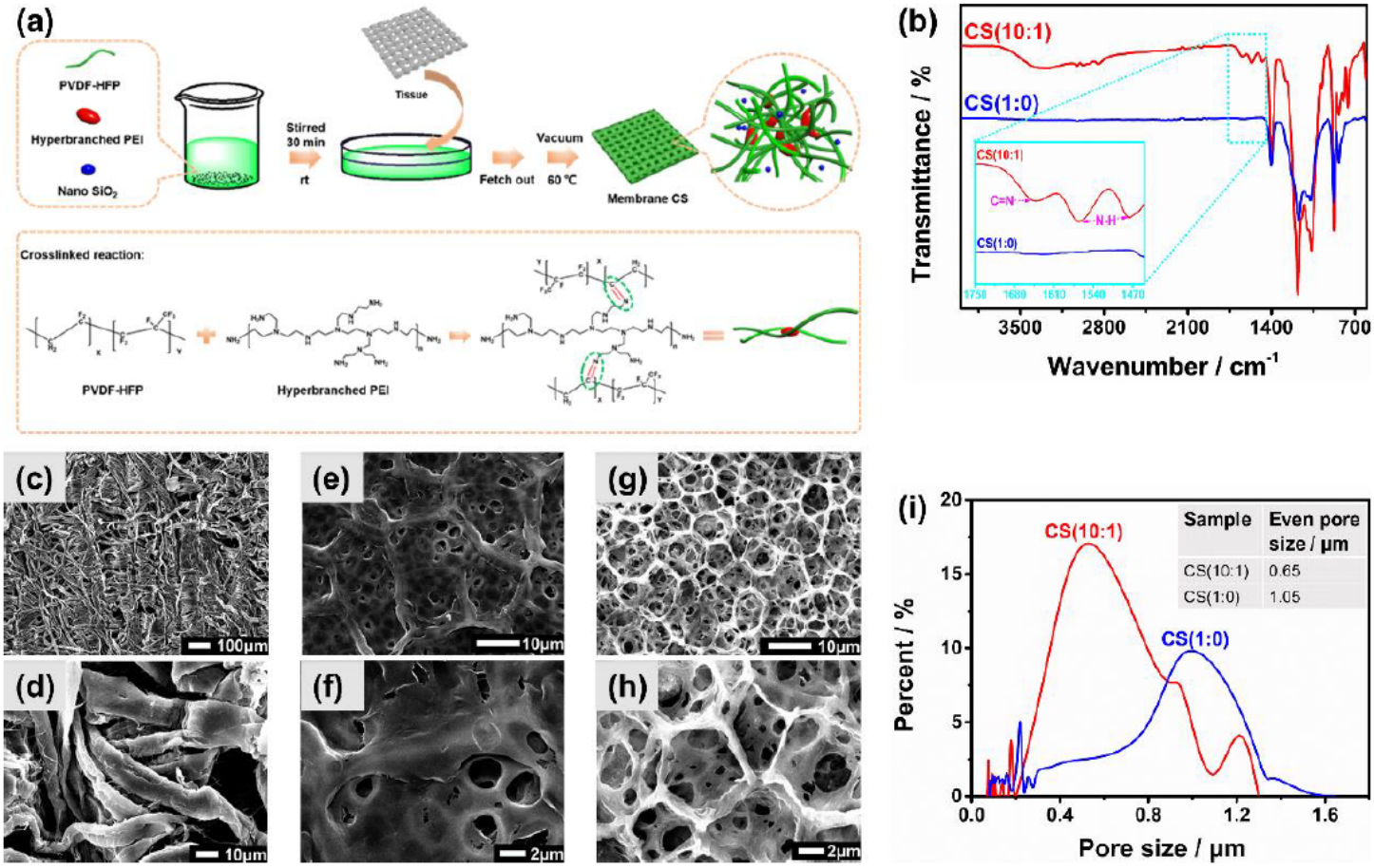

Figure 1

(a) Fabrication procedure of crosslinked layer constructed on tissue paper and crosslinking reaction process thereof; (b) ATR-FTIR spectra of CS(10:1) and CS(1:0) separator (inset: an enlarged graph at the range of 1750-1450 cm-1); SEM images of ((c) and (d)) tissue paper, ((e) and (f)) CS(1:0) separator and ((g) and (h)) CS(10:1) separator with different magnification; And (i) Pore size and distribution of CS(10:1) and CS(1:0) separator.

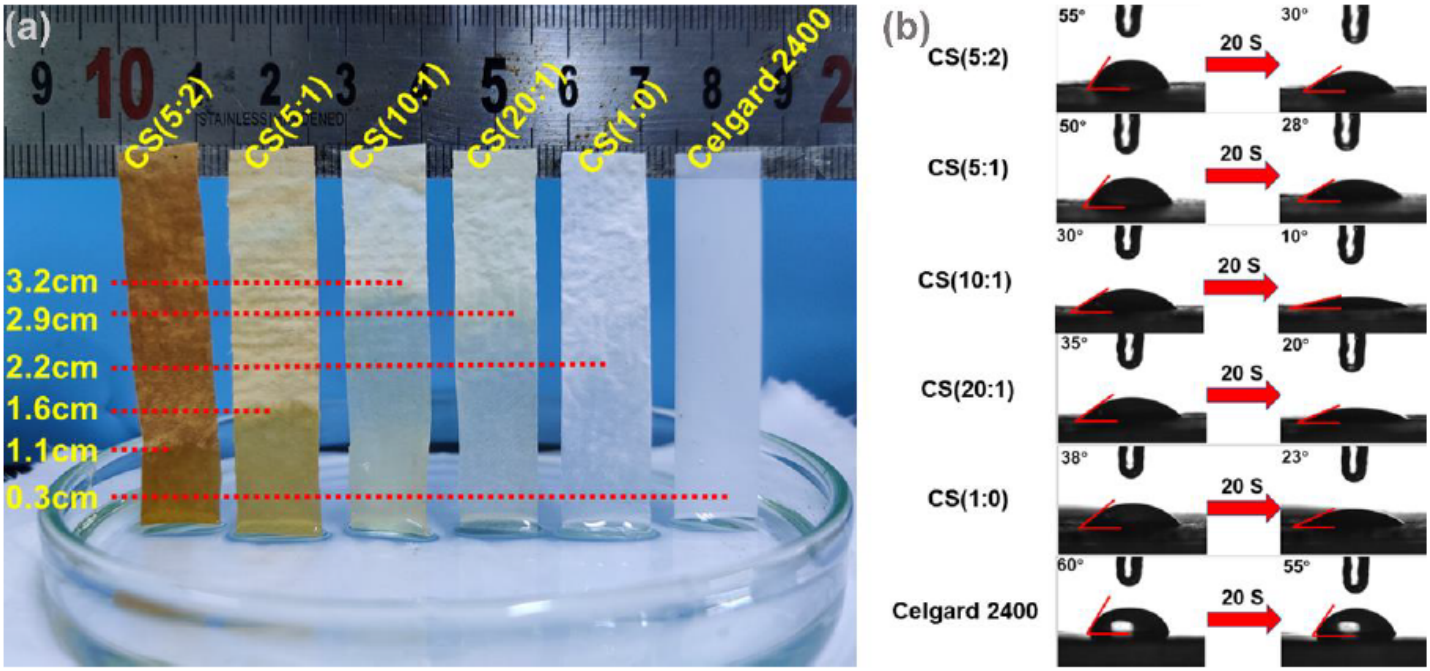

Figure 2

(a) Photograph of liquid electrolyte immersion-height after separator immersed in 120 min and (b) contact angle images of electrolyte droplet respectively on CS(5:2), CS(5:1), CS(10:1), CS(20:1), CS(1:0) and Celgard 2400 separator.

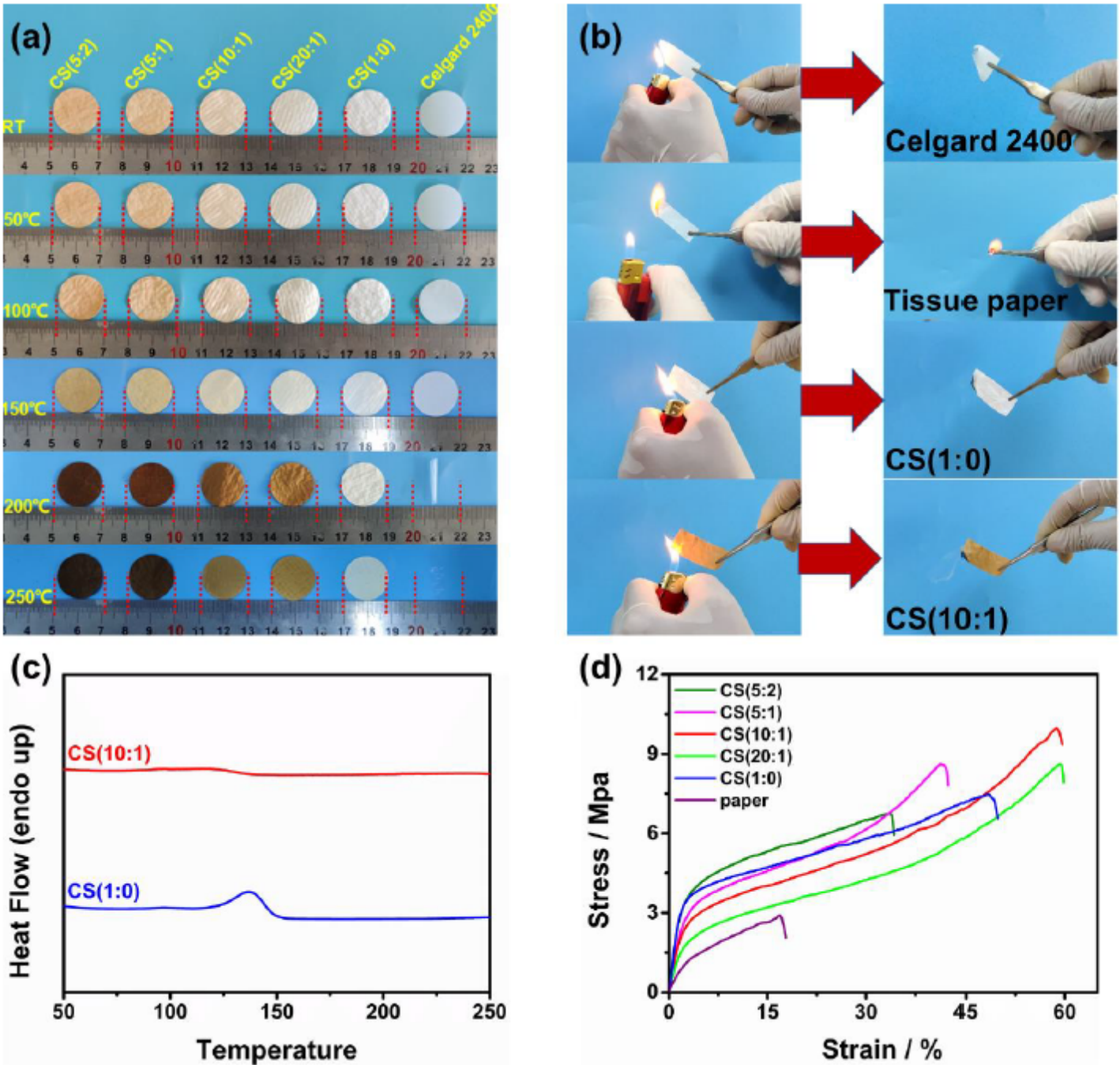

Figure 3

(a) Photographs of separators at room temperature and after thermal treatment at 50 °C, 100 °C, 150 °C, 200 °C and 250 °C for 1h respectively; (b) ignition tests of pure paper and separator Celgard 2400, CS(1:0), CS(10:1); (c) DSC curves of separator CS(10:1) and CS(1:0); (d) Stress strain curves of tissue paper and composite separators.

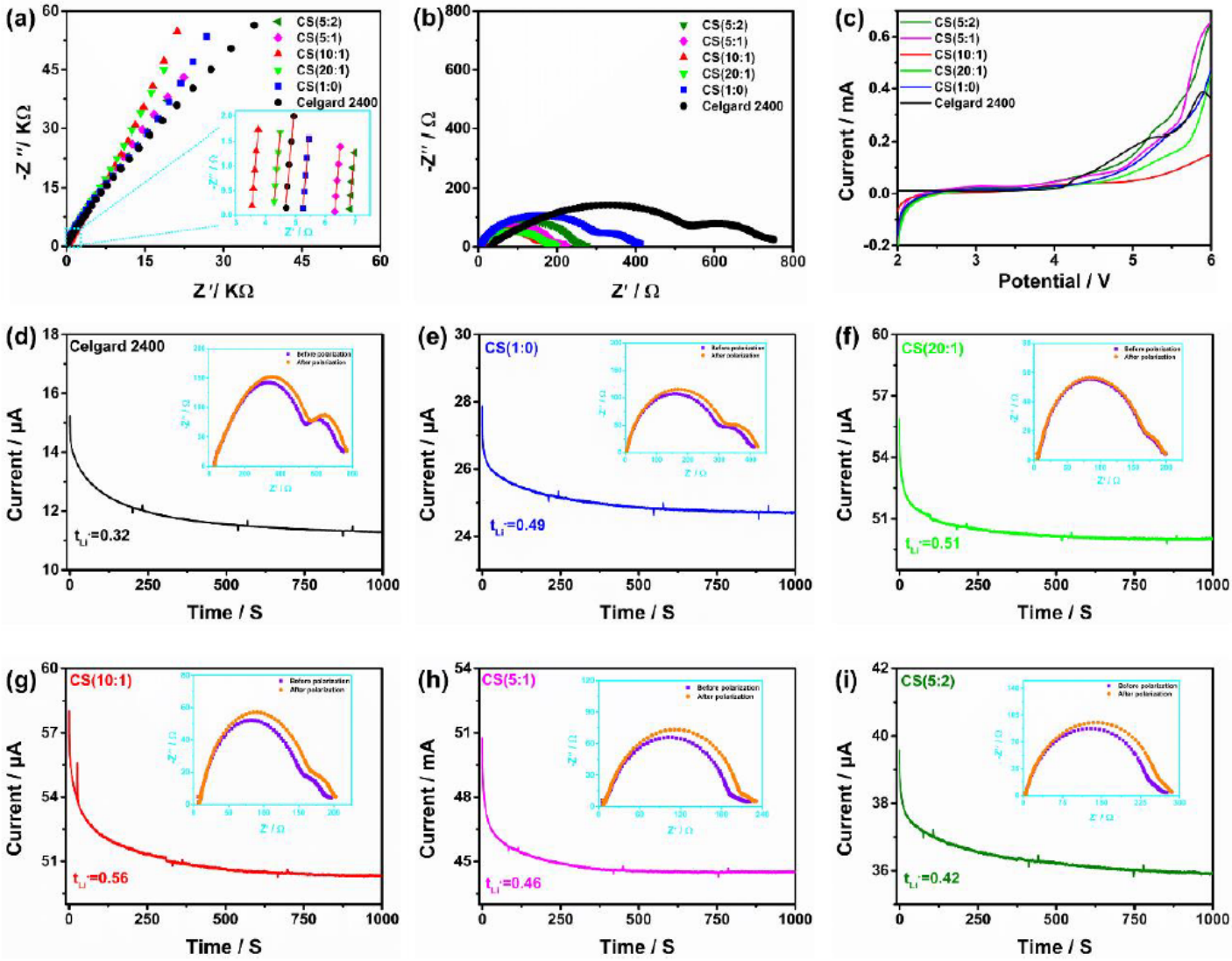

Figure 4

(a) Nyquist plots of SS/separator/SS cells respectively using CS(5:2), CS(5:1), CS(10:1), CS(20:1), CS(1:0) and Celgard 2400 as the separator; (b) interfacial impedance curves of Li/separator/Li cells with the six separators; (c) LSV curves of SS/separator/Li cells with the six separators; and (d-i) chronoamperometry of Li/separator/Li cells after applying a DC voltage of 10mV (inset: the corresponding EIS for the same cells before and after polarization).

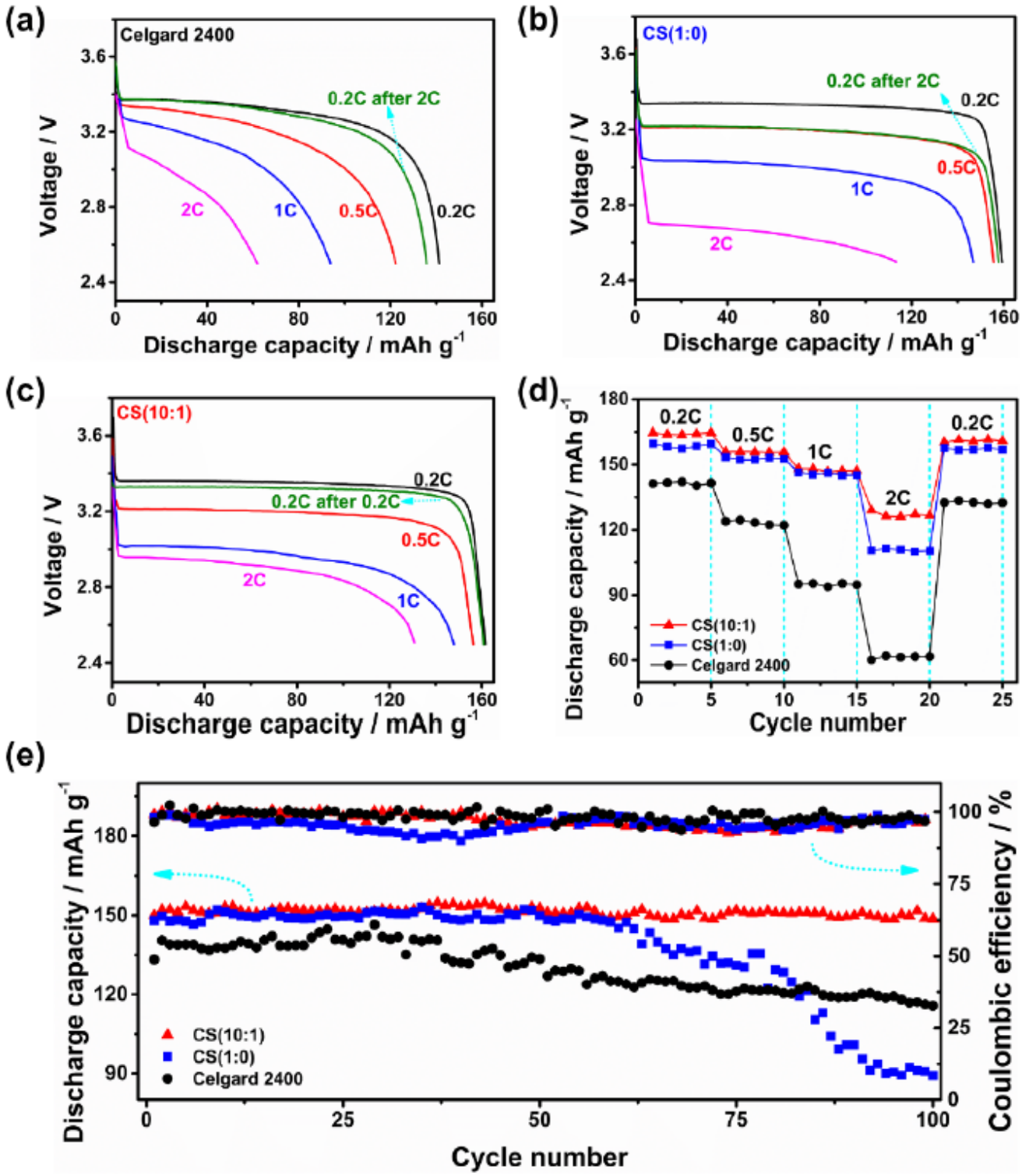

Figure 5

Discharge capacity curves of cells based on (a) Celgard 2400, (b) CS(1:0) and (c) CS(10:1); (d) summary of C-rate capabilities of cells with the different separators; and (e) Cycling performance of cells using different separators.

Supplementary Files

This is a list of supplementary files associated with this preprint. Click to download.

- GraphicalAbstract.tif
- SupplementaryMaterial.docx